CHINESE OPTICS LETTERS

Vol. 19, No. 7 | July 2021

# Ultrafast control of slow light in THz electromagnetically induced transparency metasurfaces

Yi Zhao (赵 毅)[1], Qiuping Huang (黄秋萍)[1,2*], Honglei Cai (蔡宏磊)[1], Xiaoxia Lin (林晓霞)[1], Hongchuan He (何泓川)[3], Hao Cheng (程 浩)[3], Tian Ma (马 天)[2], and Yalin Lu (陆亚林)[1,2,3**]

[1] Hefei National Laboratory for Physical Science at the Microscale, University of Science and Technology of China, Hefei 230026, China

[2] Anhui Laboratory of Advanced Photon Science and Technology, University of Science and Technology of China, Hefei 230026, China

[3] Department of Materials Science and Engineering, University of Science and Technology of China, Hefei 230026, China

*Corresponding author: qphuang@ustc.edu.cn

**Corresponding author: yllu@ustc.edu.cn

Received September 8, 2020 | Accepted December 19, 2020 | Posted Online March 30, 2021

In this paper, we experimentally demonstrate ultrafast optical control of slow light in the terahertz (THz) range by combining the electromagnetically induced transparency (EIT) metasurfaces with the cut wire made of $P^+$-implanted silicon with short carrier lifetime. Employing the optical-pump THz-probe spectroscopy, we observed that the device transited from a state with a slow light effect to a state without a slow light effect in an ultrafast time of 5 ps and recovered within 200 ps. A coupled oscillator model is utilized to explain the origin of controllability. The experimental results agree very well with the simulated and theoretical results. These EIT metasurfaces have the potential to be used as an ultrafast THz optical delay device.

**Keywords:** metasurface; terahertz; active control; slow light.

**DOI:** 10.3788/COL202119.073602

## 1. Introduction

Electromagnetically induced transparency (EIT) is a quantum interference effect that renders a medium transparent within a narrow spectral range around an absorption line[1]. Much attention has been paid to achieve the EIT-like effects in classical oscillator systems, such as coupled resonators[2,3], electric circuits[4], and plasmonic metamaterials[5–7]. These structures have an EIT-like phenomenon attributed to the Fano resonance in the structure[8,9]. Slow light is a dramatic reduction in the group velocity of light passing through the medium[10] and has an important impact on optical science, as it can enhance light–matter interactions[11,12]. In particular, it has great promise in optical communication and computation. Therefore, many metasurfaces were designed to achieve the slow light effect[13–15]. Among them, structures with EIT-like phenomena exhibit a very large group refractive index, so they have shown great promise in slowing down the group velocity of light[16–18].

For practical applications, it is desirable that the group velocity of electromagnetic waves can be actively controlled. For this purpose, a controllable EIT metasurface is an excellent candidate. Many efforts have been devoted to the tunable EIT metasurfaces[19–24] by various means, such as thermal[19,20] and optical[21,22] methods. Furthermore, Kim *et al.*[24] demonstrated electrically tunable EIT-like spectral properties by integrating single-layer graphene onto the functional unit cells. However, manipulation speed in the available work is slow. As slow light has the potential in the optical delay device, the ultrafast control of EIT-like metasurfaces and thus ultrafast modulation of slow light are desirable.

In this paper, we propose ultrafast tunable slow light metasurfaces based on a bright-bright mode coupling EIT-like structure. The unit cell of the metasurfaces consists of a gold (Au) cut wire (CW) and two Au split-ring resonators (SRRs). In order to achieve ultrafast control of slow light, we integrate $P^+$-implanted Si CW into the SRRs. Due to the intrinsic Si having a long carrier recombination life time on the order of milliseconds, the Si in our experiments is implanted with $P^+$ to produce lattice defects of Si and further reduce the carrier lifetime of Si. Compared with previous optically tunable EIT metasurfaces[21,25–27], in the work of Hu *et al.*[25], the switching time of the EIT surface under the irradiation of near-infrared pump light is 1 ns. Our EIT metasurface with $P^+$ implantation achieves much faster control of the two states (with EIT and without EIT) of the device. We experimentally demonstrate the transmission spectra of the ultrafast EIT metasurface in the terahertz (THz) range by using optical-pump THz-probe (OPTP) spectroscopy. By changing the pump–probe delay time, we demonstrate that

the group delay of THz light can be controlled in an ultrafast manner, with one switch cycle taking only 200 ps. Then, the coupled oscillator model is also used to explain the origin of the ultrafast controllability of the device. This ultrafast EIT metasurface has the potential to be used as an ultrafast THz band optical delay device.

## 2. Structure Design and Experiments

The schematic illustration of the ultrafast EIT metasurface is shown in Figs. 1(a) and 1(b). As shown in Fig. 1(b), the unit cell of the EIT metasurface consists of a CW and two SRRs, which are made of Au, and there is a CW made of $n-$Si between the CW and each SRR. The parameters of the structure are given: the length of Au CW $L = 85\,\mu$m, the width of Au CW and SRR $w = 5\,\mu$m, the side length of SRR $l = 29\,\mu$m, and the periods of the structure $P_1 = 120\,\mu$m, $P_2 = 80\,\mu$m. The size of the unit cell ensures that no diffraction happens, and thus the EIT metasurface behaves as an effective medium. The structure was fabricated on the Si-on-sapphire (SOS) wafer comprised of 600 nm thick Si and 530 $\mu$m thick sapphire, with a microscopy image shown in Fig. 1(c). Firstly, the Si layer of SOS was ion implanted with $P^+$ at a dose of $10^{13}$ cm$^{-2}$ and an energy of 100 keV. Then, the CW of Si was fabricated by the standard UV photolithography and reactive ion etching on the SOS substrate. Finally, the Au CW and Au SRRs are overlaid on the Si structure using the lift-off method.

## 3. Results and Discussions

We firstly utilized the commercial software COMSOL Multiphysics 5.2 to simulate the transmission spectra. In our simulation, the propagation of the incident electromagnetic wave is perpendicular to the surface of the structure, while the (E, H) plane is parallel to the surface of the structure, as shown in Fig. 1(a). The incident wave is generated by the port boundary conditions (in our simulation, the power of the incident wave is 1 W, and the absolute value of the corresponding electric field intensity can be calculated as $2.8 \times 10^5$ V/m), and the periodic boundary conditions are employed. The transmission coefficient $S_{21}$ can be obtained from the simulations, and the transmission $T$ is extracted by $T = |S_{21}|^2$. In our simulation, the sapphire substrate was treated as a lossless dielectric with $n_{\mathrm{Sap}} = 3.42$[21]. The permittivity of Au is described by the Drude model $\varepsilon_{\mathrm{Au}} = 1 - \frac{\omega_p^2}{\omega^2 + i\gamma\omega}$, where $\omega_p = 1.37 \times 10^{16}$ Hz and $\gamma = 4.07 \times 10^{13}$ Hz[28]. The permittivity of the doped Si can be described well by the Drude model as[29] $\varepsilon = \varepsilon_\infty - \frac{\omega_p^2}{\omega^2 + i\omega/\tau_d}$, where $\varepsilon_\infty = 11.7$, $\omega_p = \sqrt{N_{\mathrm{ini}} e^2/\varepsilon_0 m^*_{\mathrm{opt}}}$ is the plasma frequency of the unexcited Si, $m^*_{\mathrm{opt}} = (m_e^{*-1} + m_h^{*-1})^{-1} = 0.15 m_e$ is the optical effective mass of the carriers, and $\tau_d = 80$ fs is the Drude damping time[30]. Since $1/\tau_d \gg \omega$ (0.2–1.2 THz), the permittivity of the doped Si can be written as $\varepsilon \approx \varepsilon_\infty + \frac{i\tau_d\omega_p^2}{\omega} = \varepsilon_\infty + \frac{i\sigma}{\omega\varepsilon_0}$, where $\sigma$ denotes the conductivity of doped Si. To clarify the mechanism of the EIT effect, we simulated the Au CW and SRR structures separately. As shown in Fig. 2(a), the Au CW shows a resonance peak at 0.7 THz, and the SRR structure shows a resonance peak at 0.89 THz, with the corresponding electric fields shown in Figs. 2(b) and 2(c). The results show that both Au CW and SRRs can be coupled with the incident THz waves directly, meaning that these two structures are both bright modes in our design. In the EIT sample, the near-field coupling between the Au CW and SRRs excites a resonance. The destructive interference between these

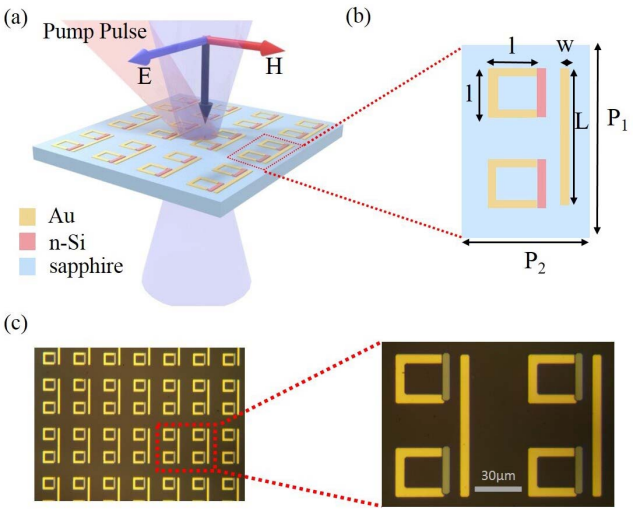


**Fig. 1.** (a) Schematic of the ultrafast EIT metasurface. (b) Parameters of structure: $P_1 = 120\,\mu$m, $P_2 = 80\,\mu$m, $L = 85\,\mu$m, $w = 5\,\mu$m, and $l = 29\,\mu$m. (c) Microscopy image of the fabricated sample.

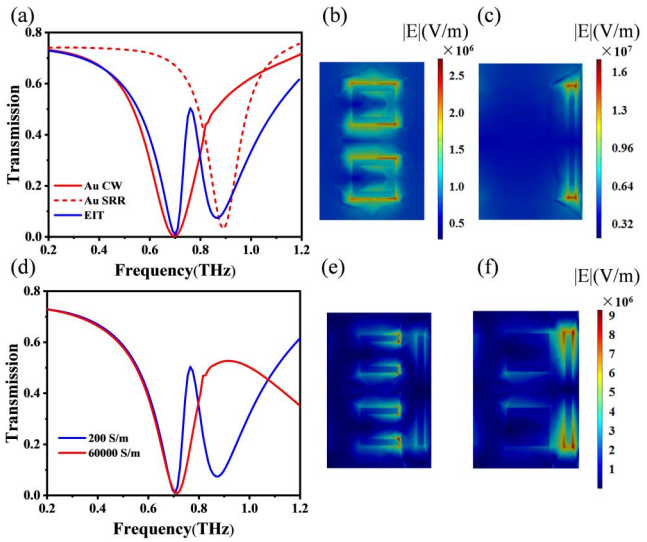


**Fig. 2.** (a) Simulated transmission spectra of Au CW, Au SRRs, and EIT sample, respectively. Electric field distribution of (b) Au SRRs at 0.89 THz and (c) Au CW at 0.7 THz. (d) Simulated transmission spectra of the EIT metasurface with different Si conductivity. Electric field distributions at 0.76 THz when Si conductivity is (e) 200 S/m and (f) 60,000 S/m (in our simulation, the absolute value of the electric field intensity of the incident wave is $2.8 \times 10^5$ V/m).

two resonances in Au CW and SRRs leads to a sharp transparency peak at 0.76 THz. Furthermore, the conductivity of Si CW is set from 200 S/m to 60,000 S/m to simulate the effect of optical excitation. In Fig. 2(d), the transmission spectrum presents an EIT peak at 0.76 THz when $\sigma_{Si} = 200\,S/m$. Figure 2(e) shows the electric field at 0.76 THz, where both the SRRs and the Au CW are simultaneously excited by the incident wave. When $\sigma_{Si} = 60{,}000\,S/m$, the electric field around the Au SRRs is completely suppressed, and the field distribution is localized at the Au CW at 0.76 THz, as given in Fig. 2(f). These results show that the EIT peak can be suppressed when carriers in Si CW are excited by the pump light.

Then, we characterized the fabricated EIT metasurface by a homemade OPTP spectrometer, with the experimental setup described in detail elsewhere[31]. The output laser pulse from a Ti:sapphire regenerative amplifier with a pulse width of 35 fs, a central wavelength of 800 nm, and a repetition rate of 1 kHz was split into three parts: two for THz generation and detection and the other one for optical excitation. THz radiation was generated by the optical rectification in a 0.5 mm thick (110)-oriented ZnTe nonlinear crystal and was focused on the sample by the off-axis parabolic (OAP) mirrors. The THz beam electric field signal is measured by the electro-optic sampling using another 0.5 mm thick (110)-oriented ZnTe crystal. The optical-pump pulse was focused on the sample with a diameter of 10 mm at an incidence angle of about 20°. The variation in the pump–probe delay was implemented using a motion stage by changing the pump beam optical path. Under various pump–probe delay, the transmitted THz pulses through the EIT metasurface and the blank sapphire reference were measured in the time domain at the pump fluence of $1.4\,mJ \cdot cm^{-2}$. The transmission spectra were obtained by performing fast Fourier transformation of time-domain signals and normalized to those of the reference. The OPTP system is shown in Fig. 3.

The differential change in the transmitted THz peak signal ($\Delta T/T$) was measured as a function of pump–probe delay, with the results shown in Fig. 4(a). It can be seen that the THz peak signal firstly reduces rapidly, resulting from the photogenerated carriers in the Si CW. Until the time delay reaches 5 ps, the THz peak signal starts to recover due to the recombination of carriers in Si. It can return to be the initial state within 200 ps.

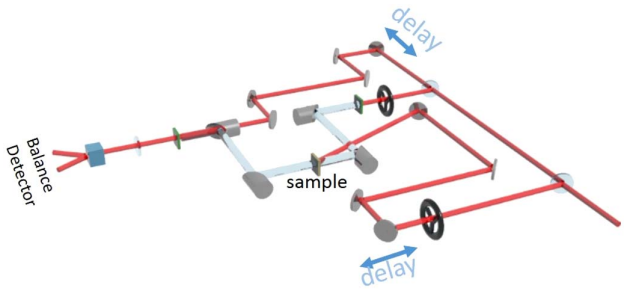


**Fig. 3.** Schematic illustration of the OPTP system. The ultrafast femtosecond laser beam is split into three beams, respectively, used for THz generation, THz detection, and ultrafast optical pump.

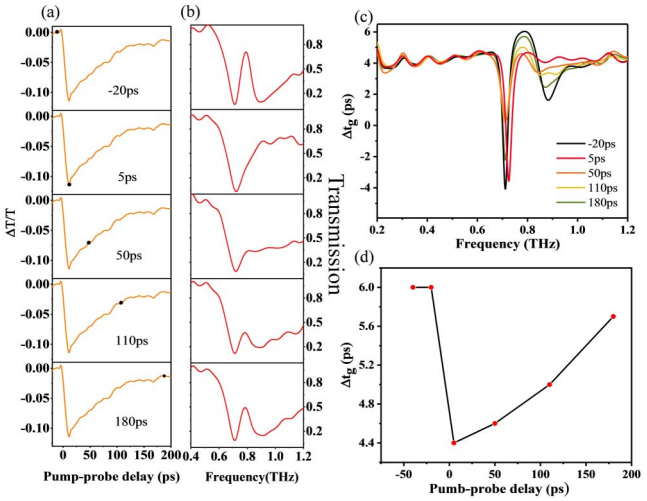


**Fig. 4.** (a) Differential change in transmitted THz peak signal as a function of pump–probe delay. Black dots indicate the specific time delay of our test. (b) Experimental transmission spectra at different time delays. (c) Time-dependent $\Delta t_g$ retrieved from measured transmission spectra. (d) Time-dependent $\Delta t_g$ at 0.78 THz.

Additionally, the transmission spectra of the EIT metasurface at different pump–probe delays are shown in Fig. 4(b). When the time delay is −20 ps, there is no photoexcitation, and the corresponding transmission spectra show an EIT peak at 0.78 THz, while the EIT peak is totally suppressed when the time delay reaches 5 ps. As the time delay increases from 5 ps to 180 ps, the EIT peak appears again. One cycle of switching from the EIT suppressing to the EIT reappearing takes within 200 ps.

In the following, ultrafast modulation of the slow light behavior is further demonstrated. The EIT metasurface changes the group refractive index by changing the dispersion of the metasurface. Since the increasing group refractive index increases the time of THz waves passing through the metasurface, the slow light effect of the metasurface can be characterized by this time value. Therefore, we use $\Delta t_g$ to describe the slow light capability of our device[21], which refers to difference in $t_g$ for THz waves to pass through the EIT metasurface and air of equivalent thickness. So, $t_g = -\mathrm{d}\varphi/\mathrm{d}\omega$, where $\varphi$ is the phase, and $\omega$ is the angular frequency of the THz pulse. The retrieved $\Delta t_g$ from the experiment is shown in Fig. 4(c). When the pump–probe time delay is −20 ps, the wave packet with a central frequency of 0.78 THz is delayed by 6 ps, which is equivalent to the time delay of a 1.8 mm free space propagation. However, when the time delay is 5 ps, the wave packet is delayed by 4 ps (caused by the substrate), which means that the EIT metasurface gradually loses its slow light characteristic. As the time delay increases to 180 ps, the slow light effect appears again. It is worth noting that there are spectral regions where the delays are negative, which would seem to allow faster-than-light wavepacket transfer. But, this phenomenon does not violate the law of causality. Superluminal group velocity can result from pulse shaping due to anomalous dispersion[32]. $\Delta t_g$ plotted as a function of pump–probe time delay at 0.78 THz is shown in Fig. 4(d).

Experimental transmission spectrum mapping as a function of pump–probe time delay is shown in Fig. 5(a) to more clearly illustrate the switching characteristics of the device. As indicated by the dashed black line, one cycle of switching on and switching off the EIT peak is within 200 ps. Additionally, to illustrate the effect of ion implantation on carrier lifetime and thus the manipulation speed of the EIT metasurface, we measured the differential change of the transmitted THz peak signal for different Si films with doping doses of $10^{13}$ cm$^{-2}$, $10^{15}$ cm$^{-2}$, and $10^{15}$ cm$^{-2}$ but annealed (rapid thermal annealing at 1000°C for 30 s), respectively. The transient differential transmission trace is fitted by a single exponential expression $\Delta T/T = A + Be^{-t/\tau}$, and the relaxation time $\tau$ is obtained, as shown in Fig. 5(b). The sample with an implantation dose of $10^{15}$ cm$^{-2}$ and without annealing presents a shorter relaxation time but a lower modulation depth than that of the $10^{13}$ cm$^{-2}$ implanted Si film and without annealing. This is due to a higher implantation dose that results in more crystal defects, which heavily reduces the carrier lifetime of Si. However, the annealing post-procession can repair the crystal defects and activate the implanted $P^+$, thus improving the carrier density and extending the carrier lifetime. So, the annealing sample has a much higher modulation depth, but much longer relaxation time. Therefore, in our experiment, a Si film with a doping dose of $10^{13}$ cm$^{-2}$ but without annealing was selected to fabricate the metasurface, taking into account that it has a good modulation depth and also a relatively short carrier lifetime.

To explain the physical origin of the EIT behavior, we use the coupled oscillator model[33] to analyze the interaction between two bright modes in the EIT structure, with the model expressed as

$$x_1'' + \gamma_1 x_1' + \omega_1^2 x_1 - \Omega^2 \exp(i\varphi) x_2 = f_1, \tag{1}$$

$$x_2'' + \gamma_2 x_2' + \omega_2^2 x_2 - \Omega^2 \exp(i\varphi) x_1 = f_2, \tag{2}$$

where $x_1$, $x_2$, $\gamma_1$, and $\gamma_2$ are the amplitudes and damping rates of the two bright modes, respectively. $\Omega^2 \exp(i\varphi)$ is the coupling coefficient between two resonators. $f_1$ and $f_2$ are the external force. Here, the discussion is only restricted to the case that $\varphi = 0$ and $f_1 = f_2 = f$. Under this condition, Eqs. (1) and (2) can be solved as

$$x_1 = \frac{\Omega^2 + (\omega_2^2 - \omega^2 - i\omega\gamma_2)}{(\omega_1^2 - \omega^2 - i\omega\gamma_1)(\omega_2^2 - \omega^2 - i\omega\gamma_2) - \Omega^4} f, \tag{3}$$

$$x_2 = \frac{\Omega^2 + (\omega_1^2 - \omega^2 - i\omega\gamma_1)}{(\omega_1^2 - \omega^2 - i\omega\gamma_1)(\omega_2^2 - \omega^2 - i\omega\gamma_2) - \Omega^4} f. \tag{4}$$

The electric current density $J$ and the surface conductivity $\sigma_e$ of the metasurface can be expressed as

$$J = -in_e\omega(x_1 + x_2) = \sigma_e E, \tag{5}$$

where $n_e$ and $E$ denote the average electron density and spatially averaged electric field on the metasurface, respectively. If assuming $f \propto E$,

$$\sigma_e = -in_e\omega \frac{2\Omega^2 + (\omega_1^2 - \omega^2 - i\omega\gamma_1) + (\omega_2^2 - \omega^2 - i\omega\gamma_2)}{(\omega_1^2 - \omega^2 - i\omega\gamma_1)(\omega_2^2 - \omega^2 - i\omega\gamma_2) - \Omega^4}. \tag{6}$$

The transmission coefficients of the metasurface can be calculated from Eq. (6):

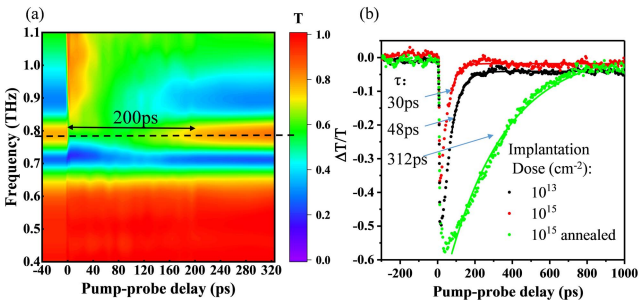


**Fig. 5.** (a) Experimental transmission spectrum mapping as a function of pump–probe delay. (b) Differential change in transmitted THz peak signal as a function of pump–probe delay for Si films with different implanted conditions. The solid curve represents the single exponential fitting with a time constant of $\tau$.

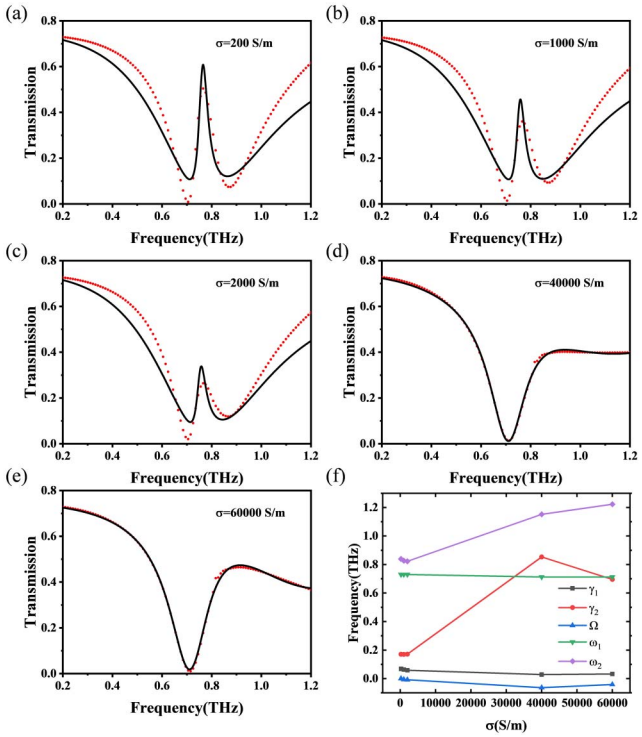


**Fig. 6.** (a)–(e) Simulated transmission spectra with Si conductivity varied between 200 S/m and 60,000 S/m (red dots) and the corresponding fitting lines (black lines). (f) The fitted parameters with different Si conductivity.

$$t = \frac{2}{2 + Z_0\sigma_e}, \tag{7}$$

where $Z_0$ is the wave impedance of the external waves.

The simulated transmission spectra with Si conductivity that varied between 200 S/m and 60,000 S/m are presented by red dotted line in Figs. 6(a)–6(e). When the Si conductivity is set to be 200 S/m, the EIT peak is activated, similar to the experimental result at −20 ps in Fig. 4(b). The EIT phenomenon is suppressed when the Si conductivity increases to 60,000 S/m, which is the same as the experimental one at 5 ps. Therefore, it can be concluded that the ultrafast manipulation of carrier density of Si CW and thus conductivity of Si contributed to the ultrafast control of the EIT peak.

The equation of $|t^2|$ is used to fit the simulation results in Figs. 6(a)–6(e), with fitted results shown by black lines in Figs. 6(a)–6(e). The fitting parameters with the Si conductivity are plotted in Fig. 6(f).

As can be seen from Fig. 6(f), $\gamma_1$ and $\omega_1$ change slightly because the Au CW resonators are hardly affected by the change of Si conductivity. A significant change in $\gamma_2$ and $\omega_2$ can be seen due to the change of Si conductivity that can affect the damping rate of the SRRs and the effective length of the electric dipole (SRRs). The value of Ω changes a little because the effective distance between these two resonators also varies a little due to the change of Si conductivity. From the above analysis, we can see that the whole process is indeed due to the ultrafast change of Si conductivity, which has a great influence on the SRRs and destroys the interference between the bright-bright mode couplings.

## 4. Conclusions

In summary, by incorporating $P^+$-implanted Si CW into the EIT metasurface unit cell, we have experimentally demonstrated an ultrafast dynamic control of slow light in THz metasurfaces. The transition from the state with the slow light effect to the state without the slow light effect occurs at an ultrafast time of 5 ps, and the recovery to the slow light effect state takes 200 ps. A coupled oscillator model has been used to explain the origin of the controllability. The ultrafast manipulation of conductivity of Si CW affects the damping rate and the effective electric dipole length of the SRRs, and thus destroys the interference between the bright-bright mode couplings. The structure we designed may be applied to an ultrafast THz band optical delay device.

## Acknowledgement

This work was supported by the National Natural Science Foundation of China (Nos. 11704373 and 51627901), Fundamental Research Funds for the Central Universities (No. WK2340000071), Open Programs for the Key Science & Technology Infrastructures of Chinese Academy of Sciences (No. CX2310000100), and Anhui Initiative in Quantum Information Technologies (No. AHY100000).

## References

1. K. J. Boller, A. Imamoğlu, and S. E. Harris, "Observation of electromagnetically induced transparency," Phys. Rev. Lett. **66**, 2593 (1991).
2. Q. Xu, S. Sandhu, M. L. Povinelli, J. Shakya, S. Fan, and M. Lipson, "Experimental realization of an on-chip all-optical analogue to electromagnetically induced transparency," Phys. Rev. Lett. **96**, 123901 (2006).
3. X. Yang, M. Yu, D.-L. Kwong, and C. W. Wong, "All-optical analog to electromagnetically induced transparency in multiple coupled photonic crystal cavities," Phys. Rev. Lett. **102**, 173902 (2009).
4. C. L. Garrido Alzar, M. A. G. Martinez, and P. Nussenzveig, "Classical analog of electromagnetically induced transparency," Am. J. Phys. **70**, 37 (2002).
5. S. Zhang, D. A. Genov, Y. Wang, M. Liu, and X. Zhang, "Plasmon-induced transparency in metamaterials," Phys. Rev. Lett. **101**, 047401 (2008).
6. N. Papasimakis, V. A. Fedotov, N. Zheludev, and S. Prosvirnin, "Metamaterial analog of electromagnetically induced transparency," Phys. Rev. Lett. **101**, 253903 (2008).
7. X. Liu, J. Gu, R. Singh, Y. Ma, J. Zhu, Z. Tian, M. He, J. Han, and W. Zhang, "Electromagnetically induced transparency in terahertz plasmonic metamaterials via dual excitation pathways of the dark mode," Appl. Phys. Lett. **100**, 131101 (2012).
8. N. Verellen, Y. Sonnefraud, H. Sobhani, F. Hao, V. V. Moshchalkov, P. V. Dorpe, P. Nordlander, and S. A. Maier, "Fano resonances in individual coherent plasmonic nanocavities," Nano Lett. **9**, 1663 (2009).
9. Y. Francescato, V. Giannini, and S. A. Maier, "Plasmonic systems unveiled by Fano resonances," ACS Nano **6**, 1830 (2012).
10. G. Heinze, C. Hubrich, and T. Halfmann, "Stopped light and image storage by electromagnetically induced transparency up to the regime of one minute," Phys. Rev. Lett. **111**, 033601 (2013).
11. T. F. Krauss, "Why do we need slow light?" Nat. Photon. **2**, 448 (2008).
12. D. M. Beggs, T. P. White, L. O'Faolain, and T. F. Krauss, "Ultracompact and low-power optical switch based on silicon photonic crystals," Opt. Lett. **33**, 147 (2008).
13. M. Lee, M. E. Gehm, and M. A. Neifeld, "Systematic design study of an all-optical delay line based on Brillouin scattering enhanced cascade coupled ring resonators," J. Opt. **12**, 104012 (2010).
14. S. Savo, B. Casse, W. Lu, and S. Sridhar, "Observation of slow-light in a metamaterials waveguide at microwave frequencies," Appl. Phys. Lett. **98**, 171907 (2011).
15. K. L. Tsakmakidis, A. D. Boardman, and O. Hess, "'Trapped rainbow' storage of light in metamaterials," Nature **450**, 397 (2007).
16. L. Zhang, P. Tassin, T. Koschny, C. Kurter, S. M. Anlage, and C. M. Soukoulis, "Large group delay in a microwave metamaterial analog of electromagnetically induced transparency," Appl. Phys. Lett. **97**, 241904 (2010).
17. C. Wu, A. B. Khanikaev, and G. Shvets, "Broadband slow light metamaterial based on a double-continuum Fano resonance," Phys. Rev. Lett. **106**, 107403 (2011).
18. J. Zhang, S. Xiao, C. Jeppesen, A. Kristensen, and N. A. Mortensen, "Electromagnetically induced transparency in metamaterials at near-infrared frequency," Opt. Express **18**, 17187 (2010).
19. C. Kurter, P. Tassin, L. Zhang, T. Koschny, A. P. Zhuravel, A. V. Ustinov, S. M. Anlage, and C. M. Soukoulis, "Classical analogue of electromagnetically induced transparency with a metal-superconductor hybrid metamaterial," Phys. Rev. Lett. **107**, 043901 (2011).
20. W. Cao, R. Singh, C. Zhang, J. Han, M. Tonouchi, and W. Zhang, "Plasmon-induced transparency in metamaterials: active near field coupling between bright superconducting and dark metallic mode resonators," Appl. Phys. Lett. **103**, 101106 (2013).
21. J. Gu, R. Singh, X. Liu, X. Zhang, Y. Ma, S. Zhang, S. A. Maier, Z. Tian, A. K. Azad, and H.-T. Chen, "Active control of electromagnetically induced transparency analogue in terahertz metamaterials," Nat. Commun. **3**, 1151 (2012).

22. F. Miyamaru, H. Morita, Y. Nishiyama, T. Nishida, T. Nakanishi, M. Kitano, and M. W. Takeda, "Ultrafast optical control of group delay of narrow-band terahertz waves," Sci. Rep. **4**, 4346 (2014).
23. S. Xiao, T. Wang, T. Liu, X. Yan, Z. Li, and C. Xu, "Active modulation of electromagnetically induced transparency analogue in terahertz hybrid metal-graphene metamaterials," Carbon **126**, 271 (2018).
24. T. T. Kim, H. D. Kim, R. Zhao, S. O. Sang, T. Ha, D. Chung, Y. H. Lee, B. Min, and Z. Shuang, "Electrically tunable slow light using graphene metamaterials," ACS Photon. **5**, 1800 (2018).
25. Y. Hu, J. You, M. Tong, X. Zheng, Z. Xu, X. Cheng, and T. Jiang, "Pump-color selective control of ultrafast all-optical switching dynamics in metaphotonic devices," Adv. Sci. 7, 2000799 (2020).
26. H. Sun, J. Yang, H. Liu, D. Wu, and X. Zheng, "Process-controllable modulation of plasmon-induced transparency in terahertz metamaterials," Chin. Opt. Lett. **19**, 013602 (2021).
27. H. Sun, Y. Tang, Y. Hu, J. You, H. Liu, and X. Zheng, "Active formatting modulation of electromagnetically induced transparency in metamaterials," Chin. Opt. Lett. **18**, 092402 (2020).
28. M. A. Ordal, L. L. Long, R. J. Bell, S. E. Bell, R. R. Bell, R. W. Alexander, and C. A. Ward, "Optical properties of the metals Al, Co, Cu, Au, Fe, Pb, Ni, Pd, Pt, Ag, Ti, and W in the infrared and far infrared," Appl. Opt. **22**, 1099 (1983).
29. N. Kamaraju, A. Rubano, L. Jian, and S. Venkatesan, "Subcycle control of terahertz wave form polarization using all-optically induced transient metamaterials," Light: Sci. Appl. **3**, e155 (2014).
30. K. Sokolowskitnten and D. V. der Linde, "Generation of dense electron-hole plasmas in silicon," Phys. Rev. B **61**, 2643 (2000).
31. H. Cai, S. Chen, C. Zou, Q. Huang, Y. Liu, X. Hu, Z. Fu, Y. Zhao, H. He, and Y. Lu, "Multifunctional hybrid metasurfaces for dynamic tuning of terahertz waves," Adv. Opt. Mater. **6**, 1800257 (2018).
32. W. Withayachumnankul, B. M. Fischer, B. Ferguson, B. R. Davis, and D. Abbott, "A systemized view of superluminal wave propagation," Proc. IEEE **98**, 1775 (2010).
33. X. Hu, S. Yuan, A. Armghan, Y. Liu, Z. Jiao, H. Lv, C. Zeng, Y. Huang, Q. Huang, Y. Wang, and J. Xia, "Plasmon induced transparency and absorption in bright–bright mode coupling metamaterials: a radiating two-oscillator model analysis," J. Phys. D: Appl. Phys. **50**, 025301 (2016).